EARTH OBSERVATION SATELLITE – 04 (EOS-04) ATBD FOR OCEAN SURFACE WIND PRODUCTS

Version 1.1

June 2024

DOCUMENT CONTROL SHEET

1.	**Date**	June 2024
2.	**Title**	Retrieval algorithm for high resolution ocean surface wind speeds using observations from the Synthetic Aperture Radar (SAR) on-board Earth Observation Satellite - 04 (EOS-04)
3.	**Doc. No.**	EOS-04 ATBD for Ocean Wind Version 1.1
4.	**Type of Report**	Technical - Algorithm Theoretical Basis Document (ATBD)
5.	**No. of Pages**	13
6.	**Authors**	Abhisek Chakraborty and Pradeep Kumar Thapliyal
7.	**Originating Centre**	Space Applications Centre (ISRO), Ahmedabad
8.	**Abstract**	An algorithm is developed for the retrieval of ocean surface wind speed products from the ISRO's second civilian synthetic aperture radar (SAR) mission on-board Earth Observation Satellite - 04 (EOS-04). The wind speed products generated using this newly developed algorithm is validated using operational wind products from Advanced Scatterometer (ASCAT) data. The validation of the EOS-04 wind speed products indicates that these products have the quality to be utilised in operational and R&D applications.
9.	**Keywords**	EOS-04, SAR, wind
10.	**Approving Authority**	Inter-centre ATBD Review Committee
11.	**Classification**	Unrestricted
12.	**Circulation**	Open

Product Name (Ocean surface wind speed)

Sr. No.	Product Code	Spatial Resolution	Temporal Resolution	Geographical Extent
1	STGCWWHTD	500 m	Scene-wise	North Indian Ocean

Brief Product Specification

Product Name	**Ocean surface wind speed**	WW
Unit	Metre per second	
Summary of Product Algorithm	High resolution ocean surface wind speed retrieved from EOS-04 C-band SAR Level-2 GeoRef data.	
Product Resolution	500 m	
Product Coverage	North Indian Ocean including BoB and AS	
Spatial Interpolation Method	-	
Time Resolution	Scene-wise	
Product Range	-	
Product Accuracy	2 m/s (RMS) or 10% whichever will be higher for wind speed ranging 4-25 m/s	

Title: High resolution ocean surface wind from C-band SAR on-board EOS-04

1.0 Algorithm Specifications:

Version	Date	Prepared by	Description
1.1	June 2024	Abhisek Chakraborty, & Pradeep Kumar Thapliyal	Level-3 ocean surface wind speed product from EOS-04 data

2.0 Introduction

2.1 Satellite and Instrument

The Earth Observation Satellite – 04 (EOS-04) which was erstwhile known as Radar Imaging Satellite -1A (RISAT-1A) was launched by the Indian Space Research Organisation (ISRO) as its second civilian Synthetic Aperture Radar (SAR) mission on February 14, 2022 carrying a C-band (5.4GHz) SAR as the sole payload. The payload is capable of imaging the earth surface in various modes viz. Stripmap, Sliding Spotlight and ScanSAR with different polarization combinations viz. Single, Dual, Hybrid and Full-pol. The C-band SAR was injected into a polar sun-synchronous orbit at 525km altitude with the equatorial crossing times a 6AM/6PM in descending/ascending nodes. For the present algorithm, we have used medium resolution (MRS) mode ScanSAR acquisitions with 160 km swath and 18 m pixel spacing covering mainly the north Indian ocean including the coastal regions.

3.0 Overview & Background

3.1 Theoretical background

A polar-orbiting side looking radar like a SAR provides the backscattering coefficient (sigma-naught, σ0) over the Earth's surface. Physically, the backscattering coefficient gives a measurement of the surface roughness. Over the oceans, the surface roughness is mainly caused by winds blowing over the surface. The local wind generates capillary waves, which are modulated by the undelaying gravity waves. The in-orbit receiver receives maximum return of the transmitted microwave signal from the capillary-gravity waves which are in resonant with the incident radar wavelength. Thus, the radar return (backscattering coefficient) from the ocean surface is directly dependent on the ocean surface winds. Such a dependency can be physically expressed in the form of the given equation (Romeiser et al., 1997)

$$\sigma 0 = 8\pi k^4 cos^4\theta \, |\alpha_{pp}|^2 [\psi(K_B, \Phi, u_{10}) + \psi(K_B, \pi - \Phi, u_{10})] \quad (1)$$

Where k is the radar wave number, θ is radar incidence angle, α is scattering coefficient dependent on transmit-receive polarization (pp) and incidence angle and Ψ is the directional

ocean wave height spectra dependent on the wind speed at 10m height (u_{10}), wind direction (Φ) relative to radar antenna and Bragg's wave number (K_B). The two terms of wave height spectra corresponds to the waves coming towards and receding away from the radar footprint.

Now, in order to retrieve wind vector (speed and direction) from σ0 observation available at each pixel, we need to invert (1) requiring a priori information of Ψ, which is not practically possible at global scale, because there are only few wave-rider buoys available over the global oceans which give accurate measurements of this parameter.

Thus, in operational scenario, the dependency of backscattering coefficient on winds and other sensor specific parameters are derived empirically in the form of a geophysical model function (GMF) which is mathematically expressed in the form of (2) as given below (Mankad et al. 2019):

$$\sigma 0 = A0(1 + A1cos\chi + A2cos2\chi + A3cos3\chi + \cdots) \quad (2)$$

Where *A0*, *A1*, *A2* and *A3* coefficients are non-linear functions of radar incidence angle and wind speed and χ is the relative azimuth representing the angle between the wind direction and antenna azimuth. The values of the coefficients can be found in Hersbach (2010) and in the references therein. It is intuitive to note that by carrying out the mathematical inversion of the GMF, information of the ocean surface winds can be retrieved from the SAR derived backscattered data.

The ocean winds retrieved from SAR are of extreme importance, as they contain very fine scale information, not available from any other space-borne sensors. For example, ocean winds very near to the coasts can only be derived accurately from SAR data. Other space-borne sensors (e.g., scatterometers, radiometers etc.) have comparatively larger footprint and the signal over such footprints is often contaminated by the presence of coastal land mass. In Fig. 1, we show an illustration depicting the importance of SAR derived surface winds for the coastal regions. Here, the SAR data is taken from Sentinel-1. Wind is retrieved from the C-band SAR onboard Sentinel-1 backscattering product using the algorithm described in this document. The interpolated ECMWF wind forecast as well as Scatsat-1 (scatteromter) acquisition are also shown in the figure. The Sentinel-1 data was acquired over the Gulf of Manner. During the time of acquisition, the tropical cyclone Burevi was prevailing in that region. It can be noted that both ECMWF forecast and Scatsat-1 were not able to capture the high winds associated with Burevi, however Sentinel-1 captured higher winds (~ 30 m/s) in comparison to Scatsat-1 or ECMWF. Another interesting fact which can be seen that Scatsat-1 with its larger (~ 30km)

footprint was not able to provide wind observations very near to the coast, whereas Sentinel-1 winds are available even very near to the coasts. Accurate estimation of ocean winds very near to the coasts help in identifying the potential locations for setting up offshore wind farms.

In addition, suitable choice of operating MW frequency make the SAR data capable of retrieving winds in extreme weather conditions like tropical cyclones and hurricanes (Horstmann et al. 2013). In fact, SAR is the most suitable space-borne Radar that can be used to measure the high-resolution winds even over the cyclone eye. Such information is extremely useful in estimating the quadrant-wise distribution of sustained wind around the cyclone eye and this important information can further lead to the improvement of the cyclone track prediction and forecasting of rapid intensification. Apart from these, there are a number of mesoscale and sub-mesoscale processes occurring at the air-sea interface, require the high-resolution information of the ocean winds. SAR derived winds have shown positive impacts when assimilated into numerical weather prediction model for hurricane track forecasting (Yu et al. 2017). Thus, SAR derived high resolution winds over the oceans are highly useful in large number of met-ocean processes.

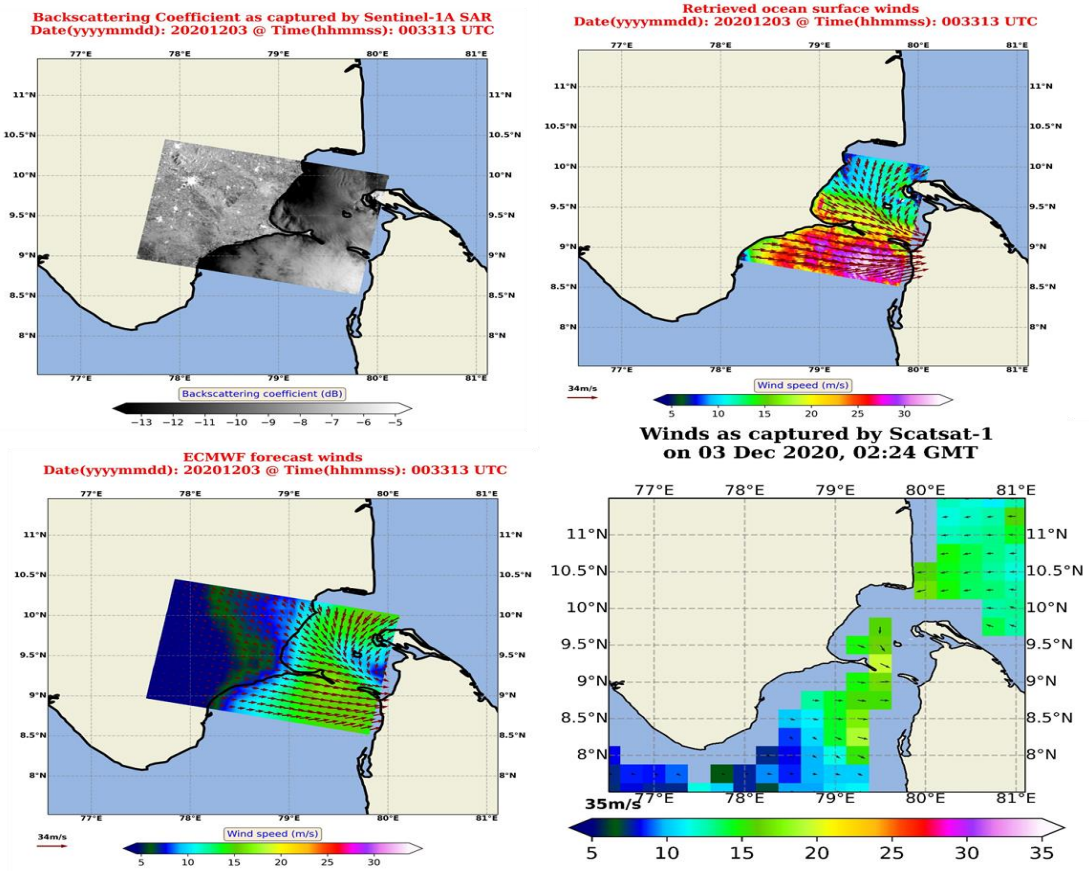

Fig. 1: *Sentinel-1A backscattering coefficient (top left panel) on 03rd December 2020. Ocean surface wind retrieved from the Sentinel-1 data is shown in top right panel (wind directions are from ECMWF). The ECMWF forecast winds interpolated over the Sentinel-1 acquisition is shown in bottom left panel. Scatsat-1 swath acquired over the region (but after a time difference of ~ 2 hours) is shown in bottom right panel.*

3.2 Indian Scenario

In Indian scenario, high resolution ocean surface wind products are generated from C-band SAR on-board RISAT-1 and EOS-04. The quality of the products have been evaluated using observations from other sensors and found to be useful for operational as well as R&D applications.

3.3 Global scenario

In global scenario, high resolution (~ 1km) ocean surface wind products are being generated using Sentinel-1 SAR data. The wind products are available from Alaska Satellite Facility (https://asf.alaska.edu/datasets/daac/sentinel-1/) and Copernicus Open Access Hub (https://scihub.copernicus.eu).

4.0 Algorithm Description

4.1 Input satellite data

Level-2 Geo referenced EOS-04 data.

4.2 Auxiliary data

Three hourly forecasts of surface met parameters of Numerical Weather Prediction (NWP) model from European Centre for Medium-Range Weather Forecasts (ECMWF).

4.3 Simulations (forward model)

For the present algorithm, we use the C-band model function version 5 derived for the equivalent neutral wind conditions (CMOD5n) (Hersbach, 2010).

4.4 Algorithm and its implementation

In this section, we provide the detailed methodology of the algorithm (Chakraborty et al., 2024) for the retrieval of ocean surface wind speed from EOS-04 SAR data. The flowchart containing the essential components of the proposed algorithm is depicted in Fig 2. In this case, we have used EOS-04 Level-2 geo-referenced data as our input. This data contains “salt-and-pepper” type noises (known as speckles) due to coherent processing of the signals. To minimize the noises, we have used Gamma Maximum A Posteriori (Gamma MAP) filter with kernel size of 5 x 5 pixels is used. Subsequently land pixels, if present in the given scene, are masked using Global Topography data available at 30 arc second (GOTPO30) resolution from United States Geological Survey (https://www.usgs.gov). Smaller islands and marine vehicles (ships, boats etc.) captured within a SAR scene make the backscattering values higher and this leads to artificial overestimation of wind over such objects. Thus, prior to the wind retrieval, we identified and removed the bright objects. To do this, we followed the algorithm as provided

by Mouche and Vincent (2019). In this algorithm, a window of 20 x 20 pixels is moved throughout the SAR scene along with a 5x5 target window at the centre of the larger window. Statistical parameters like mean and standard deviation of both the windows are computed and finally a threshold is estimated based on constant false alarm rate (CFAR) to separate the bright pixels from the background. After that, pixel-wise radiometric calibration of the data is performed using the following equation:

$$\sigma 0 = \frac{(DN^2 - N)}{K} \times \sin(IncAng)\,,\ K = 10^{(\frac{K_{dB}Beta}{10})} \quad (1)$$

Where, *DN* is the digital number representing the pixel value, and *N*, *IncAng*, $K_{dB}Beta$ are image noise bias, local incidence angle and calibration constant as provided in the metadata ("BAND_META.txt") file for each Level-2 product. After calibrating the product, the spatial sampling of the data is downscaled to produce output pixel spacing of 500m for the wind products.

Retrieval of pixel-wise ocean surface wind speed is carried out through mathematical inversion of the GMF simulations. The simulation of σ0 though GMF depends on relative azimuth estimated with respect to true north. Relative azimuth represents the difference between wind direction and sensor track (azimuth) angle, both to be measured following same convention (i.e., meteorological etc.) with respect to true north. In this study, we have used sensor heading angle information as provided in the metadata and wind direction from 3-hourly ECMWF forecast. Since ECMWF provides its forecast onto regular spatial grid with a 0.125°×0.125° spatial sampling, we need to interpolate the ECMWF data on SAR geolocation grid. Since SAR grid is much finer to the ECMWF grid, bilinear interpolation is used to map ECMWF forecast on the SAR geolocation grid. Also 3-hourly model forecasts of wind direction is interpolated on EOS-04 acquisition time. Finally, the interpolated forecasts of ECMWF wind directions are used for the inversion of the GMF.

In C-band, the GMF also known as C-band model function (CMOD) is very well established by virtue of long history of C-band observations by ERS-1/2 and ASCAT-A/B/C scatterometers. For the present study, we have used CMOD5n (Hersbach 2010) (C-band model function version 5 valid for 10-m equivalent neutral winds). All the C-band model functions are developed for only VV-polarized observations (for a range of incidence angles) because all the C-band scatterometer were flown with VV-polarized beams only. Thus, HH-polarized observations available from EOS-04 are first converted to equivalent VV-polarized

observations using a factor called Polarization ratio (PR) prior to wind retrieval. In the present study, we have utilized the PR model provided by Mouche et al. (2005).

The inversion of the GMF is carried out by computing the cost function as given by

$$F_{cost}(u,v) = \left(\frac{u-u_{NWP}}{\delta_u}\right)^2 + \left(\frac{v-v_{NWP}}{\delta_v}\right)^2 + \left(\frac{\sigma 0_{GMF}-\sigma 0_{obs}}{\delta_\sigma}\right)^2 \quad (2)$$

Where, $\boldsymbol{u}$ and $\boldsymbol{v}$ are zonal and meridional components of winds respectively used for simulating the GMF, $\boldsymbol{u_{NWP}}$ and $\boldsymbol{v_{NWP}}$ are zonal and meridional components of NWP forecast winds, $\boldsymbol{\sigma 0_{GMF}}$ and $\boldsymbol{\sigma 0_{obs}}$ are simulated (through GMF) and observed (from SAR) backscattering coefficients respectively. At each SAR scene pixel, the cost function $\boldsymbol{Fcost}$ is computed for the entire range of wind speed. The wind speed corresponding to minimum $\boldsymbol{Fcost}$ is estimated as the retrieved wind speed at that given pixel. Pixel-wise quality flags are generated for the land/ocean and are provided with wind products.

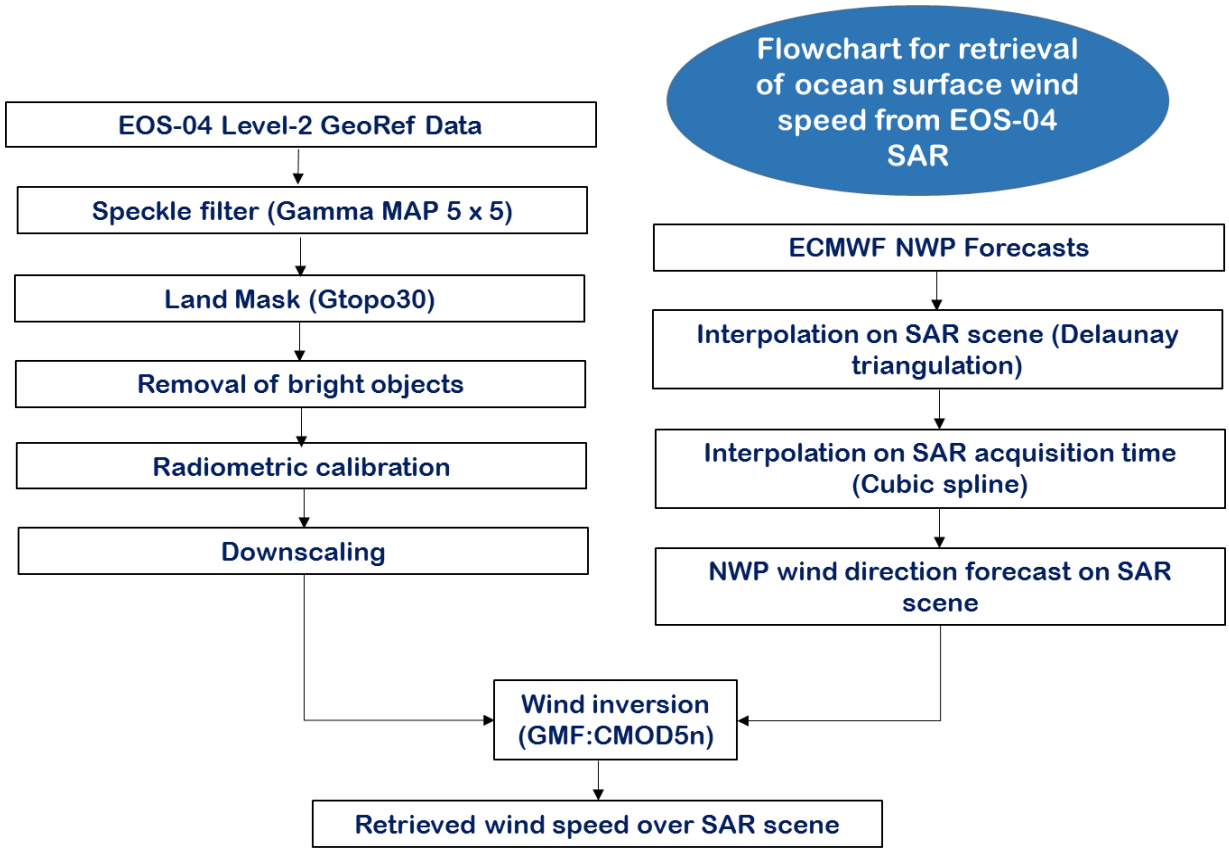

Fig 2: *Flowchart showing the algorithm to retrieve ocean winds from EOS-04 SAR data.*

A sample wind product generated from EOS-04 using the aforementioned algorithm is shown in Fig 3. The EOS-04 data was acquired over the Gulf of Kutch on 15th June 2023. In this figure, the SAR observed backscatter data and the retrieved winds are shown side-by-side. Wind directions from ECMWF forecast is also overlaid on the wind speed map. It can be noticed that EOS-04 SAR, winds could be retrieved very near to the coast, even around the small islands. This is the biggest advantage of SAR derived winds particularly for the coastal features and processes.

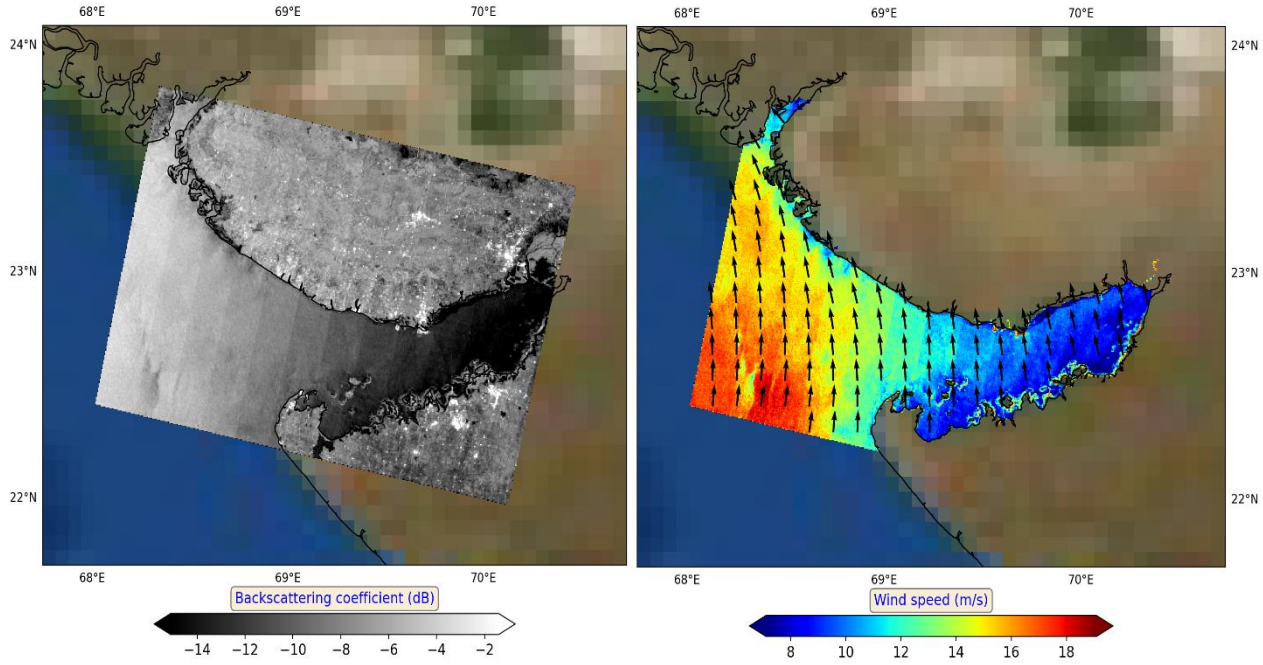

Fig 3. *Backscattering coefficient (left panel) and the retrieved winds (right panel) from EOS-04 SAR on 15th June 2023. The wind directions from ECMWF are overlaid on the wind speed map.*

5.0 Sensitivity analysis of input parameters

Prior to carrying out the evaluation of the quality of the wind products from EOS-04, we perform sensitivity analysis of various input parameters like incidence angle, azimuth angle and wind direction which is used from NWP model. Here for the forward model (i.e., CMOD5n), the wind direction and the azimuth angle are taken as a single input in the form of relative wind direction which is the wind direction with respect to antenna azimuth. In practice, both antenna azimuth (sensor heading angle in case of EOS-04) and wind direction from NWP are available in the meteorological convention (zero degree if the wind blows towards the north). Hence relative wind direction is computed as a difference between the wind direction and the antenna azimuth in modulo 360 sense. For the sensitivity analysis, we introduce error in incidence angle and relative wind direction starting from 0 (no error) to 100% in two separate cases where in each case error in only one parameter is introduced keeping others fixed. Then

errors in the retrieved wind speed is estimated with respect to the no error case. It was found that 20% error in incidence angle makes the error in wind speed more than 2 m/s which is hardly usable for any operational work. For 100% error in incidence angle, the error in wind speed becomes more than 6 m/s. On the other hand, the wind speed error in not that much sensitive to the errors in relative wind direction. It was found that 100% error in relative wind direction introduces an error of 1 m/s in wind speed.

6.0 Assessment/Validation

To evaluate the quality of the wind products generated using the aforementioned algorithm, we have validated the wind products against ASCAT operational wind products. For this purpose, we have procured ~1000 scenes of EOS-04 MRS and CRS mode data acquired in for VV and HH polarization modes during the period from December 2022 to March 2023. In Fig. 4, we show mosaic of wind speeds generated using all these SAR scenes. The speed products generated from all these SAR scenes were then collocated spatially and temporally with ASCAT wind speed data for collocation windows of 0.25º and 6 hour respectively. The scatterplot of comparison between EOS-04 and ASCAT wind speed products is shown in the right panel of Fig.4. A total number of 13,846 collocated wind speed pairs were found for the mentioned time period of four months. The wind speed bias between these two wind products was found to be negligible (-0.05 m/s). The Root Mean Square Deviation (RMSD) between the two products was found to be 1.55 m/s with a coefficient of value 0.76. This evaluation result indicates that the wind products generated from EOS-04 SAR data have the potential for utilisation in operational and research purposes.

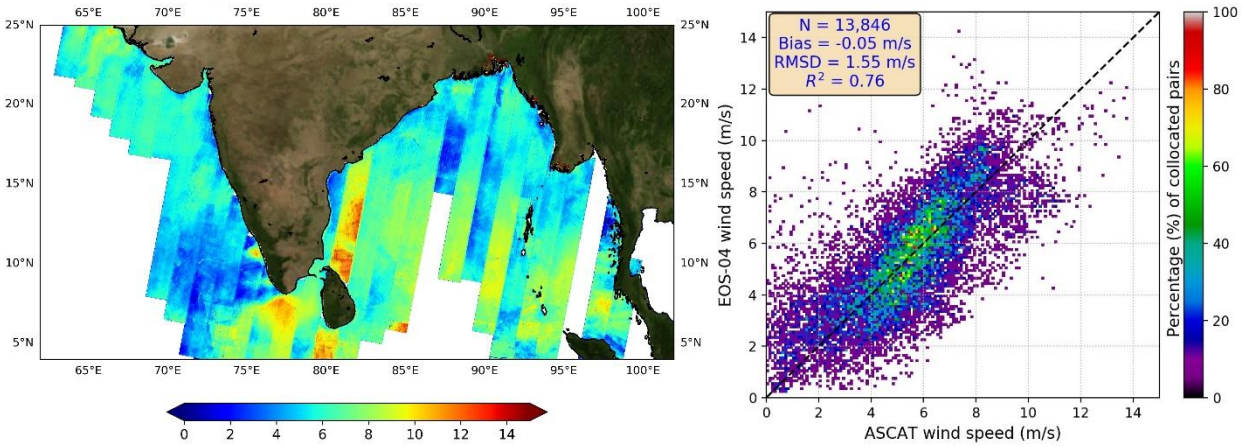

Fig 4. *Mosaic of wind fields generated from ~1000 EOS-04 scenes (left panel) and scatterplot of comparison between wind speed retrieved from EOS-04 and ASCAT (right panel) for the period from December 2022 to March 2023.*

7.0 Conclusion & Future scope

In this document, we provide detailed description of the algorithm for the retrieval of ocean surface wind speeds from the C-band SAR data available from EOS-04. The quality of the wind speeds retrieved using this algorithm is found to be good enough for various R&D and operational applications. In the nominal mode of operation, the EOS-04 is taking regular observations in descending mode over the Indian landmass as well as over the Exclusive Economic Zone (EEZ) of India. It is therefore proposed to generate scene-wise high resolution (~ 500 m) wind products for all the scenes acquired in the nominal mode operationally using the algorithm described in this document. When sufficient wind products will be available, the assessment of the winds can further be investigated using observation from coastal moored buoys (very less in numbers and need a significant number of wind products for obtaining sufficient collocation). In addition, due to larger footprint, wind products from scatterometer are not available very near to the coast with good accuracy. Thus, in future, attempts can be made to combine wind products from both SAR and scatterometer to generate seamless coastal as well as offshore wind maps.

8.0 Acknowledgments

The authors sincerely thank Shri. Nilesh M. Desai, Director, Space Applications Centre, Dr. Rashmi Sharma, Deputy Director, Earth & Planetary Sciences and Applications Area for their guidance and constant support. Dr. Neeraj Agarwal, Head Physical Oceanography Division, and NISAR Theme Coordinator for Oceans is thankfully acknowledged for several scientific discussions related to this ATBD. The members of the inter-centre ATBD review committee are gratefully appreciated for their constructive suggestions during the review of this ATBD. EOS-04 data were obtained from Bhoonidhi web portal of National Remote Sensing Centre. EUMETSAT is thankfully acknowledged for providing the ASCAT data. The NWP centre ECMWF is gratefully acknowledged for providing the model analysis data

References

Chakraborty, A., N. Sharma, N. Jaiswal, and B. P. Shukla, (2024), “Probing atmospheric phenomena using C-band Synthetic Aperture Radar on-board Earth Observation Satellite – 04”, EOS-04 Special Issue in *Current Science*, vol. 126, no. 9, pp. 1118-1125.

Hersbach, H., (2010), "Comparison of C-band scatterometer CMOD5.N equivalent neutral winds with ECMWF", *Journal of Atmospheric and Oceanic Technology*, vol.27, pp. 721 – 736.

Horstmann, J, C. Wackerman, S. Falchetti, S. Maresca (2013), "Tropical cyclone winds retrieval from synthetic aperture radar", *Oceanography*, vol. 26, no. 2, pp. 46-57.

Mankad, D., R. Sikhakolli, P. Kakkar, Q. Saquib, K. M. Agarwal, S. Gajjar, D. K. Jain, V.M. Ramanujam and P. Thapliyal, (2019), "SCATSAT-1 Scatterometer data processing", *Current Science*, vol. 117, no. 6, pp. 950 – 958.

Mouche, A. and P. Vincent, (2019), "Sentinel-1 Ocean Wind Fields (OWI) Algorithm Definition", CLS-DAR-NT-10-167.

Mouche A., D. Hauser, J-F Daloze, C. Guérin (2005), Dual-Polarization Measurements at C-Band over the Ocean: Results From Airborne Radar Observations and Comparison With ENVISAT ASAR Data, *IEEE Transaction on Geoscience and Remote Sensing*, Volume 43, 753 – 769.

Romeiser, R., W. Alpers and V. Wismann (1997), "An improved composite surface model for the radar backscattering cross section of the ocean surface 1. Theory of the model and optimization/validation by scatterometer data", *Journal of Geophysical Research*, vol. 102, C11, pp 25237 – 25250.

Yu, Y., X. Yang, W. Zhang, B. Duan, X. Cao, H.Leng (2017), "Assimilation of Sentinel-1 derived surface winds for typhoon forecasting", *Remote Sensing*, 9, 845.

== End of the document ==